PLOS GENETICS

RESEARCH ARTICLE

Comprehensive analysis of central carbon metabolism illuminates connections between nutrient availability, growth rate, and cell morphology in *Escherichia coli*

Corey S. Westfall, Petra Anne Levin*

Department of Biology, Washington University, St. Louis, Missouri, United States of America

* plevin@wustl.edu

OPEN ACCESS

Citation: Westfall CS, Levin PA (2018) Comprehensive analysis of central carbon metabolism illuminates connections between nutrient availability, growth rate, and cell morphology in *Escherichia coli*. PLoS Genet 14(2): e1007205. https://doi.org/10.1371/journal.pgen.1007205

Editor: Lotte Søgaard-Andersen, Max Planck Institute for Terrestrial Microbiology, GERMANY

Received: September 19, 2017

Accepted: January 17, 2018

Published: February 12, 2018

Data Availability Statement: All relevant data are within the paper and its Supporting Information files.

Funding: This work was supported by National Institutes of Health grants GM64671 to PAL. CSW was supported by an Arnold O. Beckman Postdoctoral Fellowship from the Arnold and Mabel Beckman Foundation. The funders had no role in study design, data collection and analysis, decision to publish, or preparation of the manuscript.

Abstract

Bacterial morphology is a complex trait that is highly sensitive to changes in the environment. For heterotrophic organisms, such as *Escherichia coli*, increases in nutrient levels are frequently accompanied by several-fold increases in both size and growth rate. Despite the dramatic nature of these changes, how alterations in nutrient availability translate into changes in growth and morphology remains a largely open question. To understand the signaling networks coupling nutrient availability with size and shape, we examined the impact of deletions in the entirety of non-essential central carbon metabolic genes on *E. coli* growth rate and cell size. Our data reveal the presence of multiple metabolic nodes that play important yet distinctive roles in dictating biosynthetic capacity and shaping cell morphology. Specifically, perturbations of acetyl-CoA metabolism impact cell size and division through changes in fatty acid synthesis. Additionally, we identify a genetic pathway linking glucose levels to cell width through the signaling molecule cyclic-AMP. Together our findings highlight a surprising diversity of factors and mechanisms contributing to growth potential and cell morphology, providing a foundation for further studies.

Author summary

Often taken for granted, the shape of bacterial cells is a complex trait that is highly sensitive to environmental perturbations. Nutrients in particular, strongly impact bacterial morphology together with growth rate. The ubiquitous, rod-shaped bacteria *Escherichia coli* increases both length and width several fold upon a shift from nutrient poor to nutrient rich medium, a change accompanied by an equally dramatic increase in growth rate. Central carbon metabolism is an obvious site for the integration of nutrient dependent signals that dictate cell size and shape. To develop a clearer picture of the molecular mechanisms coupling nutrient assimilation with cell growth and morphology, we screened the entirety of non-essential carbon metabolic genes for their contribution to growth rate and cell shape. Our data reveal the presence of multiple regulatory circuits coordinating different metabolic pathways with specific aspects of cell growth and morphology. Together,

Competing interests: The authors have declared that no competing interests exist.

these data firmly establish a role for central carbon metabolism as an environmentally sensitive sculptor of bacterial cells.

Introduction

The behavior and physiology of single celled organisms is at the mercy of their environment. Nutrients, in particular, dramatically impact the growth rate, cell cycle, and morphology of bacteria. *Salmonella typhimurium*, *Escherichia coli*, and *Bacillus subtilis* cells cultured in nutrient rich conditions exhibit mass doubling times up to 6-fold faster than their counterparts cultured in nutrient poor medium [1–3]. These increases in growth rate are accompanied by similarly dramatic increases in cell size. *E. coli* increases length (2-fold) and width (1.5-fold) for a ~3-fold increase in the 2D micrography square area between nutrient poor and nutrient rich conditions [3]. *B. subtilis* increases length ~3-fold in nutrient rich conditions while width remains more or less constant [2,4].

The positive relationship between nutrient availability, growth rate and cell size is generally referred to as the "Growth Law". Besides cell size, DNA, RNA, and protein content of the cell also show a positive relationship with growth rate, with faster growing cells containing more of these macromolecules [1]. Although there is more total DNA/RNA/protein in larger, faster growing cells, their concentration remains relatively constant due to the concomitant increase in cell size [1,5].

Despite its name, the relationship between growth rate and cell size is complicated and there are several, well known exceptions to the Growth Law. Reducing growth rate by lowering culture temperature does not impact cell length or width, suggesting that it is nutrients rather than growth rate that determine cell size [6]. Conversely, mutations that lead to modest delays in division frequently result in increases in cell length without detectably impacting mass doubling time [7–9]. In support of a more nuanced situation, recent work supports the presence of a General Growth Law, at least in *E. coli*, in which cell mass at replication initiation and cell cycle duration contribute to individual cell size in addition to overall growth rate [10].

Central carbon metabolism: A hub connecting nutrient availability with growth rate and cell size

As the entry and processing point for the raw materials required for cell growth and proliferation, central carbon metabolism (CCM) plays a key role in coordinating nutrient availability with cell growth and size. Recent work indicates that CCM impacts bacterial morphology in several ways: by its impact on cell cycle progression [11–13]; by its impact on lipid synthesis [6]; and through its impact on cell wall biogenesis [14]. Genetic links between CCM and respiration and cell morphology have also been identified by high-throughput image analysis [15] [16].

CCM-mediated changes in cell cycle progression primarily affect cell length, while changes in lipid synthesis and cell wall biogenesis impact both length and width. In an example of the former, UDP-glucose, produced in two steps from glucose-6-phosphate at the beginning of glycolysis, stimulates interactions between the moonlighting glucosyltransferase OpgH in *E. coli* and the unrelated enzyme UgtP in *B. subtilis* and the essential tubulin-like cell division protein FtsZ, delaying division and increasing cell length during growth in carbon rich medium [4,13]. In contrast, defects in fatty acid synthesis (FAS) lead to reductions in both length and width, effectively recapitulating the impact of nutrient limitation on cell morphology [6,17].

CCM can also affect morphology via its impact on the availability of cellular building blocks, particularly those required for synthesis of the cell wall. In a recent study, the Young laboratory determined that defects in *wecE*, a gene encoding an aminotransferase important for making the *E. coli* outer membrane molecule enterobacterial common antigen (ECA), led to the formation of swollen, filamentous cells. ECA is transported to the cell wall via undecaprenyl-phosphate, the lipid carrier responsible for shuttling precursors for peptidoglycan and other components of the bacterial cell envelope across the plasma membrane. Careful genetics revealed the morphological defects associated with defects in *wecE* were due to sequestration of undecaprenyl-phosphate conjugated to an ECA intermediate, interfering with peptidoglycan synthesis [18].

More generically, nutrient starvation leads to an accumulation of the small molecule guanosine tetraphosphate (ppGpp) that interacts directly with RNA polymerase, to inhibit transcription of a wide array of genes, effectively curtailing flux through multiple biosynthetic pathways [19]. ppGpp concentration is inversely proportional to both size and growth rate: ectopic expression of the ppGpp synthetase RelA during growth in nutrient rich medium reduces both growth rate and cell size [6,20]. The reduction in size is indirect and dependent on ppGpp-mediated inhibition of fatty acid synthesis, while the reduction in growth rate is almost certainly a consequence of ppGpp-dependent inhibition of a host of essential processes [6].

While these examples highlight several ways in which CCM might impact the positive relationship between cell growth and cell morphology, they represent only a small fraction of the pathways that constitute CCM. To identify additional connections between nutrient levels, metabolism, and cell size in *E. coli*, we screened non-essential (CCM) gene deletions for defects in cell size and growth rate. Our data highlight three CCM nodes—the first branch-point of glycolysis, the pentose-phosphate pathway, and acetyl-CoA metabolism—as critical links between nutrient availability, cell growth and cell size. While some aspects of CCM bottlenecks appear to directly impact the relationship between nutrient availability and biosynthetic flux, other aspects of CCM effect growth and morphology in more nuanced ways.

Results

Multiple connections exist between CCM, growth rate, and cell size

To identify key steps of CCM that impact the growth and morphology of *E. coli*, we phenotypically analyzed cells defective in 44 non-essential CCM genes (S1 Table). These experiments took advantage of the Keio Collection, an ordered insertion-deletion library of all non-essential genes in *E. coli* [21] and Coli-Inspector, an Image J plug in designed for high throughput analysis of bacterial morphology [22]. Prior to analysis, the Keio insertion-deletions were transduced into the laboratory wild type strain MG1655. Briefly, single colonies of each mutant were picked and cultured under nutrient rich conditions (Luria-Bertani (LB) broth supplemented with 0.2% glucose) to an OD_{600} of ~0.2. Cultures were then back-diluted to OD_{600} of 0.01 and tracked for 4 generations until they reached a maximum OD_{600} of 0.2 (the low OD_{600} ensures cells are all actively growing and at approximately the same growth phase prior to analysis). Cells were sampled, fixed, and imaged by phase contrast microscopy. Cell size (length and width) was determined using Coli-Inspector in ImageJ.

Based on size and mass doubling time, we assigned the 44 mutants into six classes (Table 1). Represented by two mutations, Class I cells had square areas (length x width) >10% smaller than wild type cells with mild to undetectable changes in growth rate (within 20% of wild type mass doubling time). Eight mutations fell into Class II: small (more than 10% decrease in square area than wild type) with a significant decrease in doubling time (>20% wild type). Class III was heterogenous, consisting of a population dominated by smaller than normal cells

Table 1. CCM deletion mutants exhibiting significant alterations in growth rate and/or morphology.

Gene Name	Doubling time (per minute)	Length (microns)	Width (microns)	Area (square microns)	Pathway
Wild Type	22	5.0	1.04	5.1	
Class I (Small with doubling times <20% from WT)					
sucC	25	4.6	1.02	4.6	TCA Cycle
gnd	21	4.6	1.03	4.6	Pentose-Phosphate
Class II (Small and doubling times >20% from WT)					
crr	27	4.0	1.08	4.4	Glycolysis
aceE	34	3.0	0.99	2.9	Glycolysis/Acetate/Fatty acid/TCA
tktA	33	3.6	1.01	3.7	Pentose-Phosphate
pgl	26	4.4	1.03	4.5	Pentose-Phosphate
rpiA	28	3.8	1.01	3.8	Pentose-Phosphate
rpe	37	3.1	0.99	3.1	Pentose-Phosphate
pta	33	3.2	0.94	3	Acetate Metabolism
ackA	36	2.7	1.01	2.7	Acetate Metabolism
Class III (Short and Long)					
acnB	25	5.5	1.02	5.6	TCA Cycle
zwf	30	4.4	0.98	4.4	Pentose Phosphate
Class IV (Long)					
yggF	19	6.4	1.05	6.7	Putative Gluconeogensis
talB	23	5.5	1.06	5.8	Pentose-Phosphate
eda	22	5.8	1.04	6	Entner-Douderoff
Class V (heterogenous)					
tpiA	30	ND	ND	ND	Glycolysis
gpmM	21	ND	ND	ND	Glycolysis

Each strain was grown in LB-glu to an OD-600 ~0.1 and a minimum of 200 cells were measured.

https://doi.org/10.1371/journal.pgen.1007205.t001

and punctuated by the presence of a few (5–10%) very long cells. Three mutants fell into Class IV long (>10% longer than WT) and two into Class V, heterogeneous with a wide distribution of cell lengths and variable cell widths (Fig 1A). Surprisingly, the majority of mutants (26) were essentially wild type with regard to growth rate and cell size (Class VI). This finding suggests the presence of alternative pathways that permit *E. coli* to bypass particular CCM enzymes and/or that nutrients that allow for bypass are present in LB. We elected not to investigate the impact of deletions in either *ppsA*, the first step of gluconeogenesis, or *fumC*, one of the three isoforms involved in the conversion of fumarate to malate in the TCA cycle, on cell size as we were unable to obtain stable MG1655 transductants of either mutant. Representative images of each mutant are shown (Fig 2).

Notably, differences in size between CCM mutants are primarily due to reductions in cell length, rather than cell width (Table 1). This phenomenon is apparent when one compares the aspect ratio (length/width) of different strains. The aspect ratio of short mutants (e.g. *aceE*::*kan*) is less than that of wild-type cells (3.0 vs. 4.8), while the aspect ratio of long mutants (e.g. *yggF*::*kan*) is considerably larger than wild-type (6.1 vs. 4.8). In contrast, because both width and length both vary positively with nutrient availability, the aspect ratio of wild type cells remains more or less constant during growth across different nutrient conditions (S1 Fig).

To ensure that fixation was not affecting our cell size data, we measured both MG1655 and *aceE*::*kan* cells both prior to and subsequent to fixation. While fixation tended to reduce cell length to a small extent (3.5 to 3.4 μm^2 for MG1655 and 1.8 to 1.5 μm^2 for *aceE*::*kan*), the

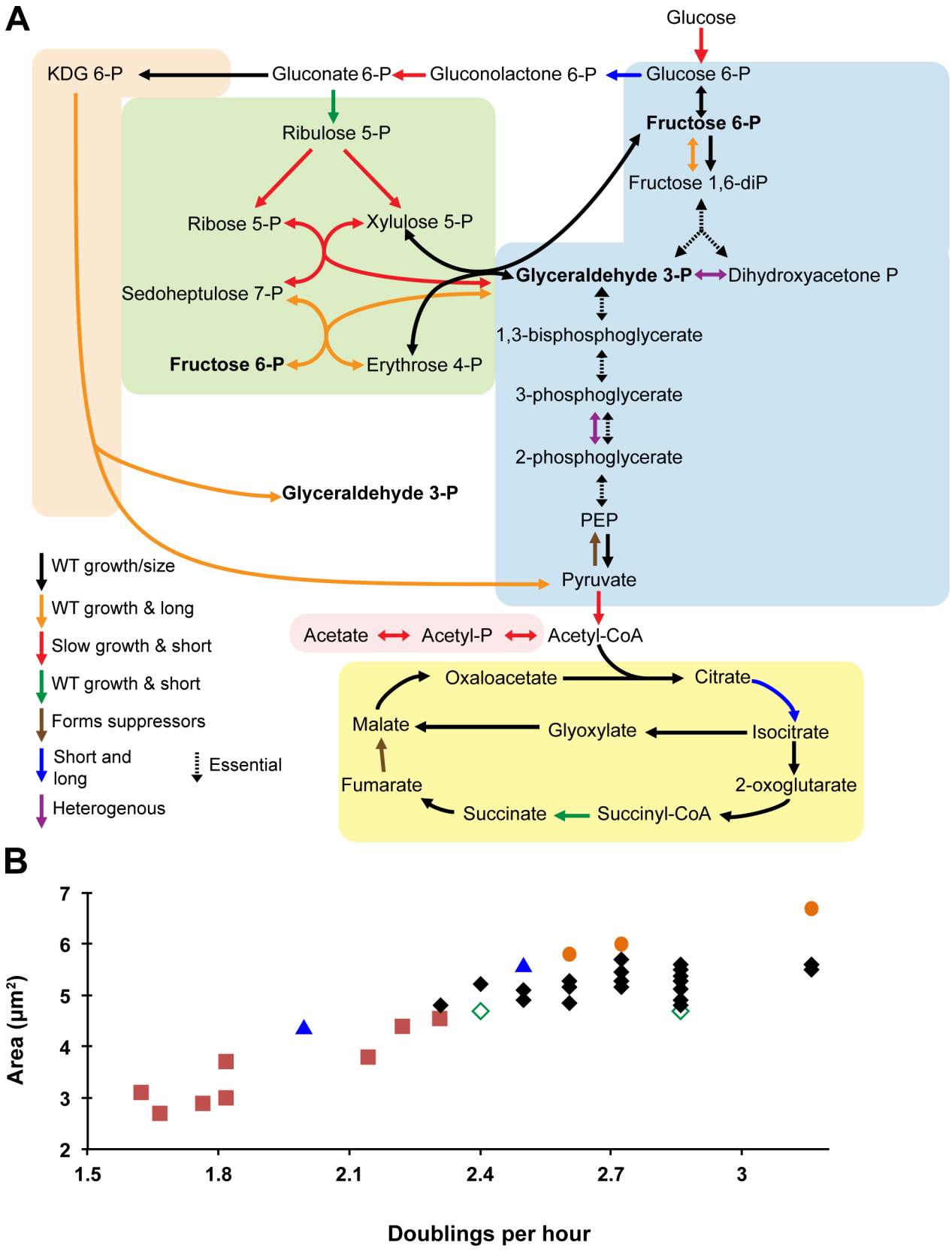
A
Glucose
KDG 6-P
Gluconate 6-P
Gluconolactone 6-P
Glucose 6-P
Fructose 6-P
Fructose 1,6-diP
Ribulose 5-P
Ribose 5-P
Xylulose 5-P
Sedoheptulose 7-P
Fructose 6-P
Erythrose 4-P
Glyceraldehyde 3-P
Dihydroxyacetone P
1,3-bisphosphoglycerate
3-phosphoglycerate
2-phosphoglycerate
PEP
Pyruvate
Glyceraldehyde 3-P
Acetate
Acetyl-P
Acetyl-CoA
Oxaloacetate
Citrate
Isocitrate
2-oxoglutarate
Succinyl-CoA
Succinate
Fumarate
Malate
Glyoxylate
WT growth/size
WT growth & long
Slow growth & short
WT growth & short
Forms suppressors
Short and long
Heterogenous
Essential
B
Area (μm²)
Doublings per hour
7
6
5
4
3
2
1.5
1.8
2.1
2.4
2.7
3

Fig 1. The effect of central carbon metabolic gene deletions on cell growth and size. (A) Mutant phenotypes mapped onto central carbon metabolic pathways. Arrows are colored based on the phenotype as follows: black = normal growth and size; green = normal growth and small size (<10% smaller than WT); red = slow growth (>20% increase in doubling time) and small size; orange = normal growth and long cells (>10% larger than WT); blue = short and long cells; purple = highly variable size; and dotted lines = essential genes. Brown arrows correspond to deletions that obtained suppressor mutations rapidly and were not analyzed. Pathways are shaded as following: glycolysis/gluconeogenesis is blue, pentose phosphate pathway is green, Entner-Doudoroff is orange, acetate fermentation is red, and the TCA cycle is yellow. (B) Relationship between cell area and growth rate, as doublings per hour. Icons are colored as in panel (A).

https://doi.org/10.1371/journal.pgen.1007205.g001

difference between fixed and unfixed cells was not statistically significant, and most importantly, did not impact the relative difference between MG1655 and *aceE*::*kan* cell (S2 Fig).

Of the different classes, only the eight Class II mutants "obeyed" the Growth Law, with reductions in growth rate accompanied by predictable reductions in cell size (Fig 1B). The close correlation between growth rate and size for Class II mutants suggests that the loss of individual genes and/or their product's catalytic function, leads to a biosynthetic bottleneck that recapitulates the impact of nutrient starvation on cellular physiology. In contrast, despite their heterogeneity with regard to cell length, both Class I and Class IV mutants exhibited more or less normal growth rates, suggesting a potential defect in the signal transduction pathways coordinating CCM with cell growth and cell size. The heterogeneity of Class III and Class V indicate a loss of proper regulation of cell cycle progression and/or width control, leading to stochastic variations in cell morphology. Histograms of the class III mutants are shown in (S3 Fig).

Growth in carbon poor medium largely eliminates morphological differences between wild-type and CCM mutants

To clarify the impact of nutrient flux on individual CCM mutant phenotypes, we assessed the growth rate and size of Class I-V mutants in three different media: LB + 0.2% glucose; the minimal media AB + 0.2% glucose; and AB + 0.2% succinate. These growth conditions represent high nutrient conditions, low nutrient, glycolytic conditions, and low nutrient, gluconeogenic conditions respectively. As cells grown in minimal media tended to aggregate, cell dimensions were measured using the MATLAB software package SuperSegger, which facilitates the rapid analysis of large numbers of clumped cells [23]. In general, SuperSegger results corresponded with the Coli-Inspector data reported above, although cell areas were smaller overall likely due to a difference in how the two programs define cell boundaries and at what point of the cell cycle that they distinguish the parent cell from the resulting two daughter cells (see wild type area in Table 1 and S3 Table).

The majority of the CCM mutants retained a positive relationship between nutrient availability and cell size. During growth in carbon poor and/or gluconeogenic conditions, the areas (Fig 3) and lengths (S4 Fig) of Class I and Class II mutants approached that of wild type, particularly in AB-succinate medium, and the heterogeneous phenotype exhibited by mutants in Class III was largely relieved. Width also decreased with nutrient availability, although to a more modest extent (S5 Fig). The average width of CCM mutants ranged from 0.70–0.84 microns during growth in LB-glu and 0.56–0.69 microns during growth in AB-suc.

The size difference—both length and width—of cells defective in *ackA* or *pta*, both required for acetate fermentation, is comparatively minimal between LB-glu and AB-glu (2.1 to 1.9 μm^2 and 2.0 to 1.8 μm^2 for *pta* and *ackA* respectively) (Fig 3D), but apparent between AB-glu and AB-suc (1.9 to 1.3 μm^2 for *pta* and 1.8 to 1.3 μm^2 for *ackA*). The differential impact of growth in AB-glu and AB-suc on cell size is most easily explained by two factors: 1) aerobic acetate generation is highest in rich medium, rendering the size of *ackA* and *pta* mutants largely insensitive to nutrient rich conditions [24], and 2) acetate is not appreciably synthesized under

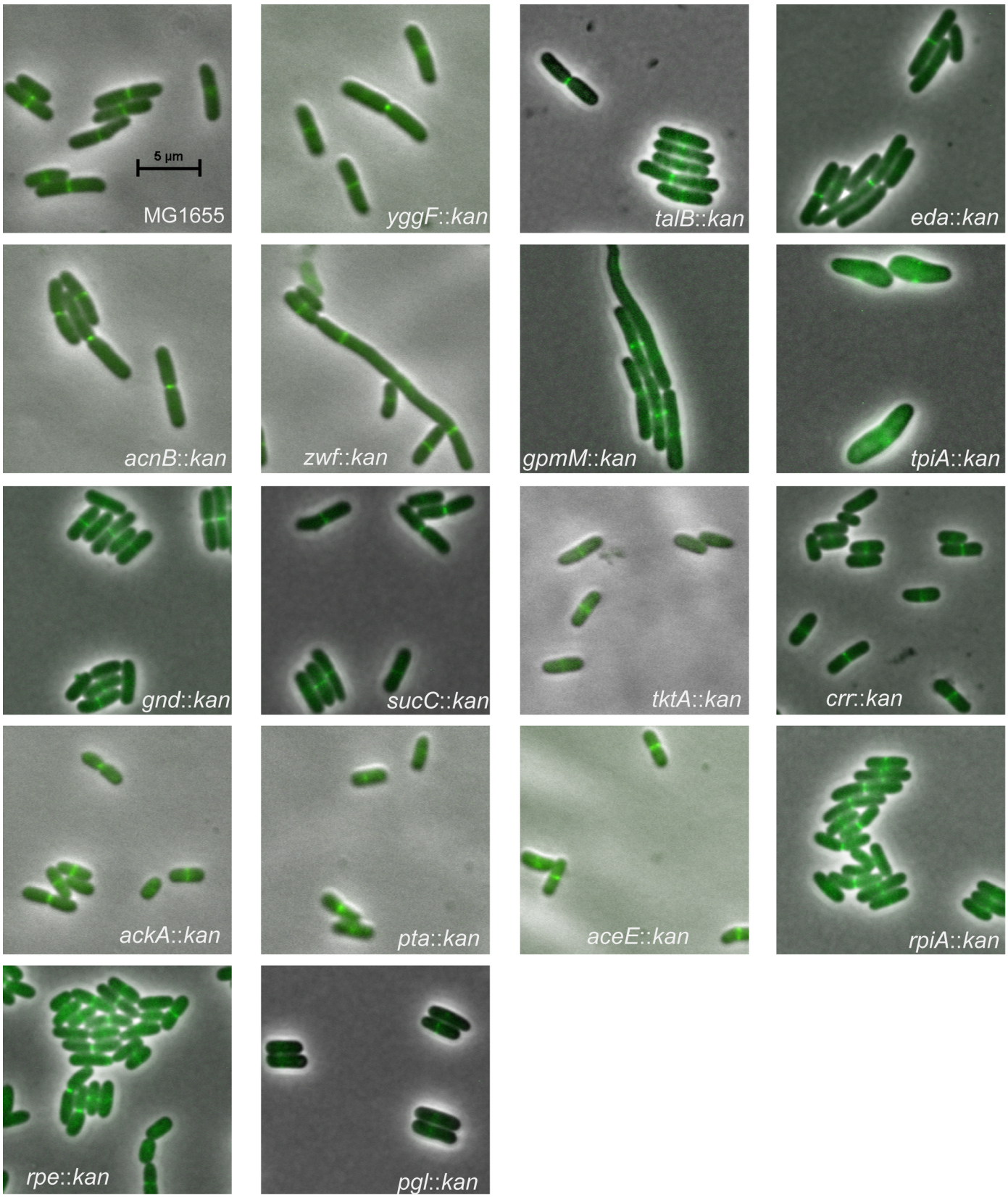
5 µm
MG1655
yggF::kan
talB::kan
eda::kan
acnB::kan
zwf::kan
gpmM::kan
tpiA::kan
gnd::kan
sucC::kan
tktA::kan
crr::kan
ackA::kan
pta::kan
aceE::kan
rpiA::kan
rpe::kan
pgl::kan

Fig 2. Representative images of all CCM mutants exhibiting morphology distinct from the wild type parental strain. Merged images of morphologically distinct CCM mutant strains expressing an *ftsZ-GFP* fusion to permit visualization of the cytokinetic ring. Cell were grown in LB-glu with 1 mM IPTG to an OD-600~.01 and fixed before visualization. Scale bar = 5 microns and is the same for all images.

https://doi.org/10.1371/journal.pgen.1007205.g002

gluconeogenic conditions, thus these mutants are expected to respond nearly identically to wild type cells during growth in AB-suc.

Although we were able to obtain cell size data for *rpiA*, *crr*, *rpe*, and *sucA* in carbon rich (LB-glu) and carbon poor (AB-glu) conditions, all four mutants were unable to grow in the gluconeogenic condition, AB + 0.2% succinate. At first glance this finding appears to be in conflict with data indicating that *rpiA*, *rpe*, and *sucA* are capable of growth in another carbon poor gluconeogenic condition: M9 + 0.1% glycerol [25]. However, this discrepancy likely reflects the ability of glycerol to enter the CCM partway through glycolysis—as dihydroxyacetone phosphate—while succinate enters through the TCA cycle, leading to dependence on different pathways through CCM to synthesize all needed carbon metabolites. The *aceE* deletion was the only CCM mutant unable to grow in either AB-glu or AB-suc, most likely due to its requirement for acetate as a precursor for acetyl-CoA synthesis [26].

In light of the significant reduction in size associated with defects in in *crr*, encoding the phosphotransferase system subunit $EIIA^{glc}$ (Table 1), we also examined the nutrient dependent phenotype of cells defective for adenylate cyclase or the cAMP receptor (Crp) production. Crr is part of a phosphodependent transferase system that is essential for the import of glucose and other sugars into *E. coli* [27]. Crr facilitates glucose import via transfer of a phosphate group from Hpr to $EIIB^{glc}$ and finally to glucose, generating glucose-6-phosphate at the beginning of glycolysis (reviewed in [28]). During growth on a non-glycolytic substrate, phosphorylated $EIIA^{glc}$ accumulates and activates the adenylate cyclase, CyaA, leading to synthesis of cyclic-AMP (cAMP) [29,30]. A co-activator, cAMP binds to Crp, promoting DNA binding at specific promoters and stimulating transcription of a broad swathe of genes including those involved in the transport and utilization of non-glycolytic carbon sources [31,32]. If *crr* impacts cell size via its impact on cAMP production and Crp activation, defects in both *cyaA* and *crp* should be phenotypically identical to *crr* mutants with regard to cell size and growth rate. We found that this is indeed true as deletions in *crr*, *cyaA*, or *crp* resulted in similar growth rates (29, 29, and 28 minutes) and cell size (2.1 square micron area for all three mutants). The similarity between the three mutants implies that the growth rate and size defect associated with *crr*::*kan* are a direct result of defects in cAMP synthesis and signaling, rather than a consequence of changes in glucose import.

Consistent with catabolite repression contributing to cell morphology, the cell area of *crp*::*kan* and *cyaA*::*kan* mutants was only modestly reduced upon a shift from LB-glu to AB-glu (Fig 3E). *crr*::*kan* mutants exhibited a significantly reduced cell area during growth in AB-Glu, but this reduction is likely a consequence of the loss of glucose import in the absence of PTS Enzyme, IIAGlc. The width of *cyaA*::*kan* and *crp*::*kan* was nearly identical in LB-glu and AB-glu, further supporting a key role for cAMP in regulating cell width (Fig 3F). This phenomenon will be addressed later in the text. *crr*, *cyaA*, and *crp* are all essential under gluconeogenic conditions, preventing analysis of these mutants in AB-succinate.

Defects in CCM differentially impact assembly of the cell division machinery

To gain insight into the relationship between growth rate, cell cycle progression and CCM during growth in LB-glucose, we assessed the ability of different mutants to suppress the heat sensitivity associated with the GTP binding defective FtsZ mutant, *ftsZ84* (G105S) [33]. While

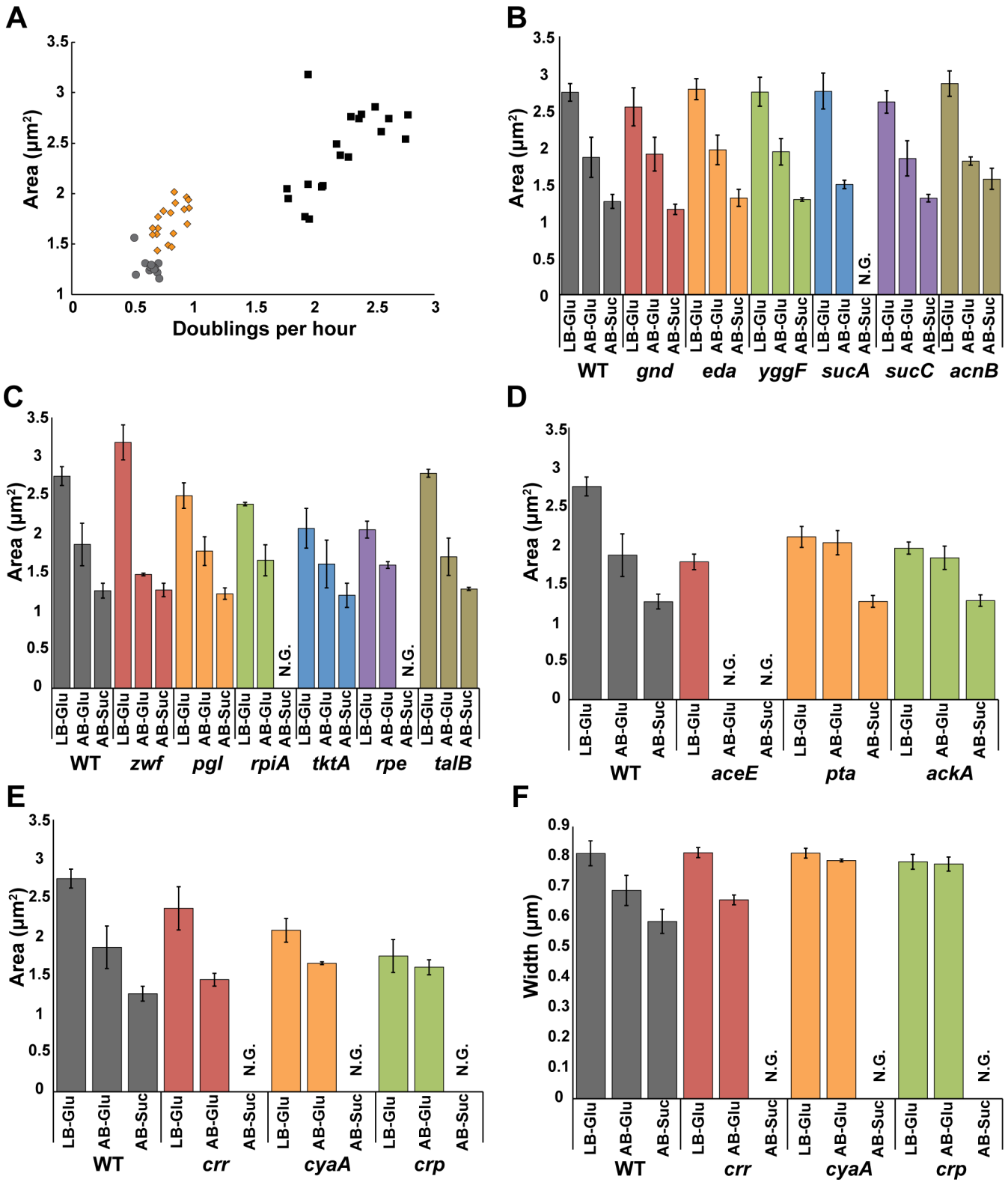

Fig 3. CCM deletions exhibit medium-dependent effects on growth and morphology. (A) Average cell area of mutants versus growth rate in LB-glucose (black diamonds), AB-glucose (orange triangles), and AB-succinate (grey circles). (B) Average area of cells grown in LB-glu, AB-glu, and AB-suc for the CCM size mutants involved in the Entner-Doudoroff, gluconeogenesis, and TCA pathways, (C) pentose phosphate pathway, (D), acetate fermentation, (E) and cAMP synthesis. (F) Nutrient dependence of average cell width of mutants defective for cAMP synthesis. Wild-type MG1655 data is shown in each panel to

aid in comparison. For each mutant/growth condition experiment, a minimum of 200 cells was measured for each of the three biological replicates. The mean is shown with error bars representing the standard error of the mean. N.G. represents no growth.

https://doi.org/10.1371/journal.pgen.1007205.g003

ftsZ84 supports both FtsZ assembly and division under permissive conditions (LB at 30˚C), under non-permissive conditions (LB with no salt at 42˚C), FtsZ assembly and division are blocked, leading to filamentation and cell death [7,34]. Based on extensive work from our group and others, conditions or mutations that enhance FtsZ assembly are expected to suppress the heat sensitivity of temperature sensitive *ftsZ* alleles [4,20,35,36]. Changes in the availability of CCM products or components that normally inhibit FtsZ assembly should restore growth and colony formation to *ftsZ84* mutants under non-permissive conditions while defects in CCM-related factors that normally promote FtsZ assembly will enhance *ftsZ84* heat sensitivity. Double mutants in CCM deletions and *ftsZ84* were generated to examine the impact of these mutants on FtsZ assembly.

Consistent with a positive impact on FtsZ assembly, the majority of Class I-V mutants promoted growth of *ftsZ84* cells under mildly restrictive conditions (37˚C, LB no salt) (Fig 4A). The strongest suppressors were loss-of-function mutations in *aceE* or *ackA* both of which increased *ftsZ84* cell viability 10,000-fold during growth at 37˚C on salt-free LB medium. Mild suppression was observed in loss of function mutations in *crr*, *tktA*, and *pta* which increased *ftsZ84* cell viability 1,000-fold, 100-fold, and 100-fold respectively. The *zwf* deletion was alone in leading to enhancement of *ftsZ84*, i.e. lack of growth at 30˚ on LB-no salt (Fig 4B). Combined with the short and long phenotype of *zwf*::*kan*, it appears that loss of *zwf* leads to impairment of FtsZ activity. Significantly, we did not observe a consistent correlation between reduced growth rate and suppression of *ftsZ84* heat-sensitivity among the various CCM mutants.

As part of these experiments we also revisited the impact of a loss of function mutation in *pgm*, encoding phosphoglucomutase—the enzyme that converts glucose-6-phosphate to glucose-1-phosphate. In previous work, we had reported that deletions in *pgm* suppress *ftsZ84* heat sensitivity [13]. However, we were unable to detect any suppression of *ftsZ84* by *pgm* in this instance. Resequencing BH173, the strain employed in the original study revealed acquisition of a reversion mutation that restored *ftsZ84* sequence to wild type.

To gain a better understanding of the mechanisms coordinating central carbon metabolism with cell morphology, we undertook an in depth analysis of two distinctive phenotypes: the reduction in length and width observed in cells defective in catabolite repression and the link between acetate metabolism, cell growth and cell cycle progression revealed by defects in *aceE*, *ptaA*, *and ackA*. The results of these efforts are described below.

Catabolite-dependent regulation of FtsZ assembly and function

Reasoning that if the product of *crr*, $EIIA^{glc}$, was impacting division indirectly via its role in stimulation of adenylate cyclase and subsequent activation of the Crp transcription factor, we hypothesized that 1) defects in either the adenylate cyclase (encoded by *cya*) or *crp* should restore growth to *ftsZ84* cells under non-permissive conditions, and 2) the addition of extracellular cAMP (which is able to diffuse through the membrane [37]) to *crr*::*kan ftsZ84* cells should bypass *crr*::*kan* mediated suppression of *ftsZ84* heat sensitivity but only in the presence of Crp. Consistent with this model, deletion of either *cya* or *crp* phenocopied *crr*::*kan* mediated *ftsZ84* suppression at 37˚C on salt free medium (Fig 5). More directly, 5 mM cAMP was sufficient to restore heat sensitivity to *crr*::*kan ftsZ84* cells as well as cells defective in adenylate cyclase (*cyaA*) but only in the presence of *crp* (Fig 5). Together, these data strongly argue for the presence of at least one inhibitor of FtsZ assembly within the extensive Crp regulon.

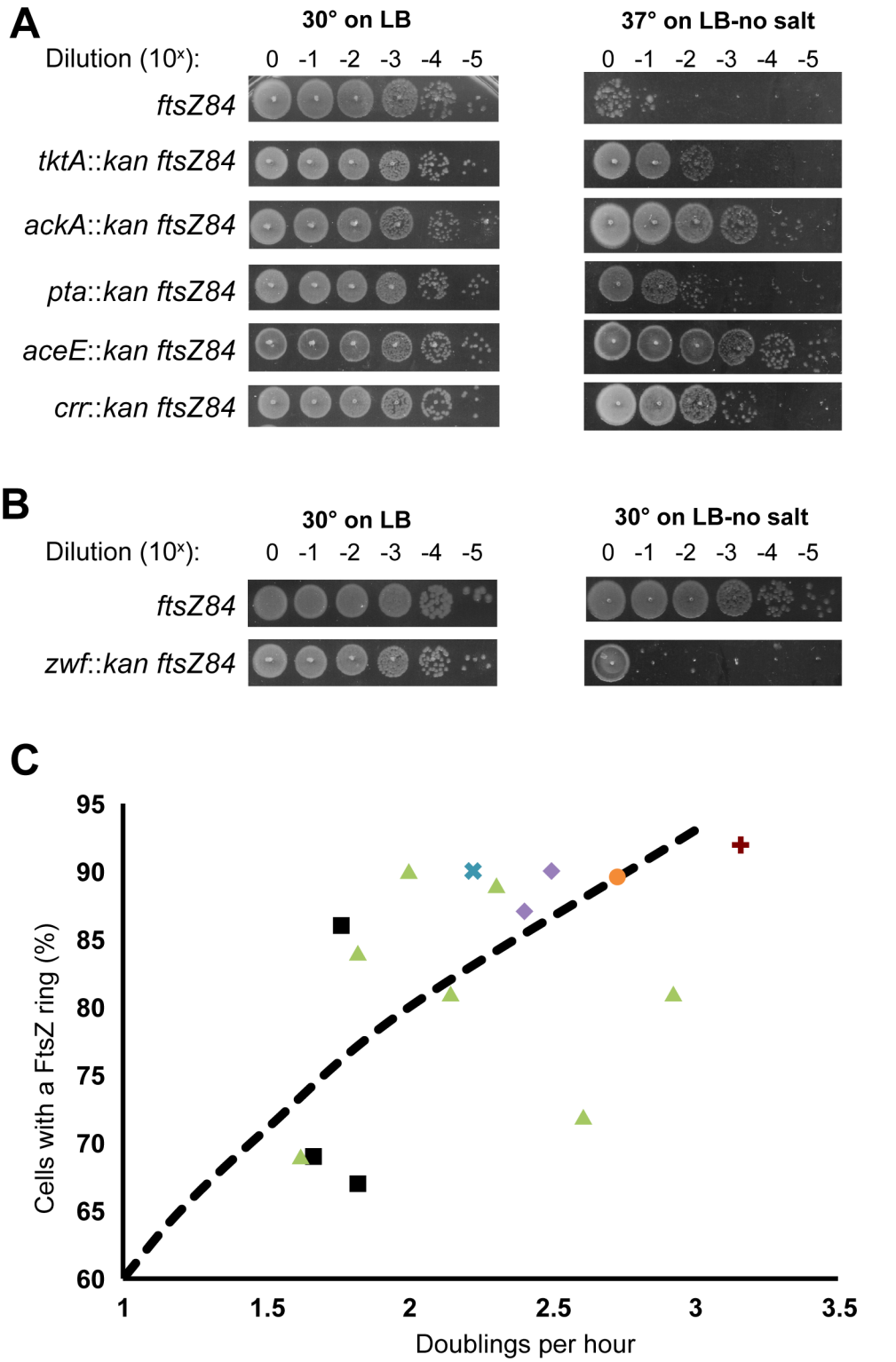

Fig 4. CCM mutations differentially impact FtsZ localization and activity. (A) Dot-plating efficiencies of the CCM deletion *ftsZ84* double mutants cultured under permissive (LB, 30˚C) and non-permissive (LB-no salt, 37˚C) conditions. Plating efficiencies were repeated three times with representative images shown. (B) Dot-plating efficiency of *zwf*::*kan ftsZ84* double mutant. Note the reduction in *zwf*::*kan ftsZ84* viability under intermediate growth conditions (30˚C on LB-no salt). Plating efficiencies were repeated three times with representative images shown. (C) FtsZ ring frequency versus growth rate for the CCM mutants. For reference we have included previously reported data on the

relationship between nutrient availability and FtsZ ring frequency (dotted black line) [13]. Mutants are grouped by metabolic pathway: black squares = acetyl-CoA production and acetate fermentation; green triangles = pentose-phosphate shunt; purple diamonds = TCA cycle; orange circle = Entner-Doudoroff pathway; blue cross = cAMP synthesis; and red plus = gluconeogenesis. Each point represents three biological replicates of at least 200 cells measured per experiment.

https://doi.org/10.1371/journal.pgen.1007205.g004

cAMP controls cell width through regulation of the morphogene *bolA*

In contrast to wild type cells, which decrease in both length and width upon a shift from glycolytic (low cAMP) to gluconeogenic (high cAMP) conditions, the *crp* deletion showed no significant changes in width when changing media from LB-glu to AB-glu, suggesting a potential role for cAMP in cell width regulation (Fig 3). To explore this idea, we examined the impact of extracellular cAMP on wild type (MG1655) cells cultured in both glycolytic and gluconeogenic conditions.

Consistent with a negative impact on cell width, 5 mM exogenous cAMP was sufficient to decrease wild type cell width in both LB and AB + 0.2% glucose (0.96 to 0.81 microns and 0.73 to 0.68 microns respectively) (Fig 6A). The addition of cAMP also significantly decreased cell length (3.8 to 3.2 microns for LB and 2.7 to 2.5 microns for AB-Glu) and growth rate (2.7 to 2.3 doubling per hour for LB and 0.98 to 0.88 doublings per hour for AB-Glu) (Fig 6B). Significantly, cAMP-dependent changes in size are not positively correlated with growth rate. Reducing levels of exogenous cAMP from 5 mM to 1 mM decreased the growth rate of *cyaA*::*kan* (which is unable to synthesize any cAMP) in gluconeogenic conditions (AB + 0.2% succinate) from 0.87 to 0.79 doublings per hour, while cell width increased from 0.65 to 0.75 microns (Fig 6C). Although width was independent of growth rate, length was not as the *cyaA*::*kan* mutant length decreased with lower cAMP from 2.6 microns in 5 mM cAMP to 2.2 microns in 1 mM cAMP in a manner similar to the growth rate (Fig 6D).

cAMP has been implicated in the Crp dependent activation of the transcription factor OmpR, which inhibits expression of a host of genes, including several whose products have morphogenic activity [38]. Of particular interest is *bolA*, encoding a transcription factor that

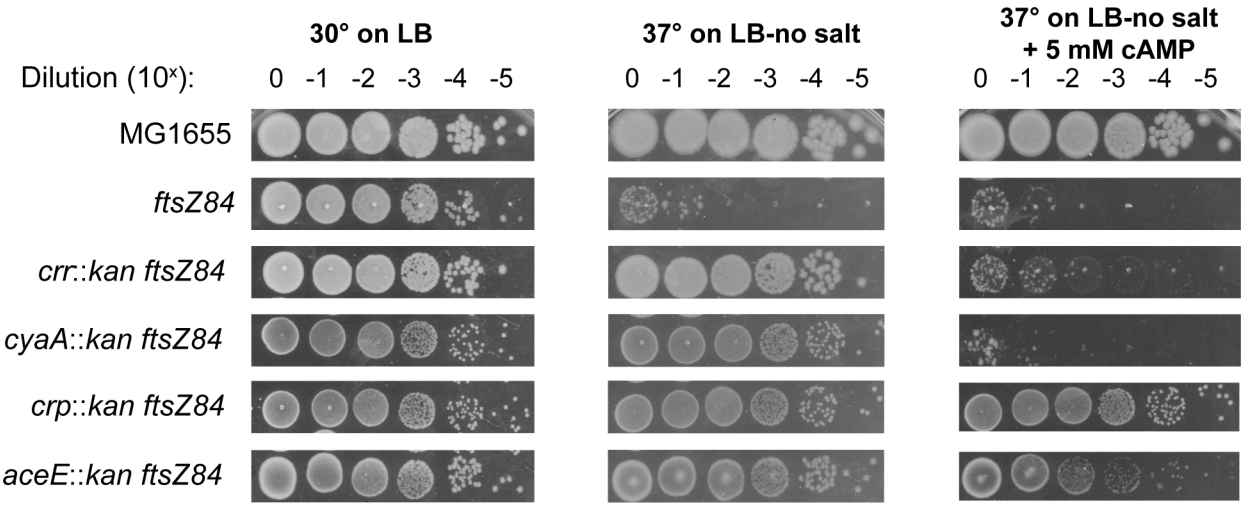

Fig 5. Loss of cAMP signaling suppresses *ftsZ84* heat-sensitivity. Representative dot-plating efficiencies of *ftsZ84* alone or in combination with insertion deletions in cAMP signaling genes *crr*, *cyaA*, and *crp*. Cells were plated on and grown at permissive (LB, 30˚C), non-permissive (LB-no salt, 37˚C), and non-permissive containing exogenous cAMP (LB-no salt + 5mM cAMP, 37˚C) conditions. Plating efficiencies were repeated three times with representative images shown.

https://doi.org/10.1371/journal.pgen.1007205.g005

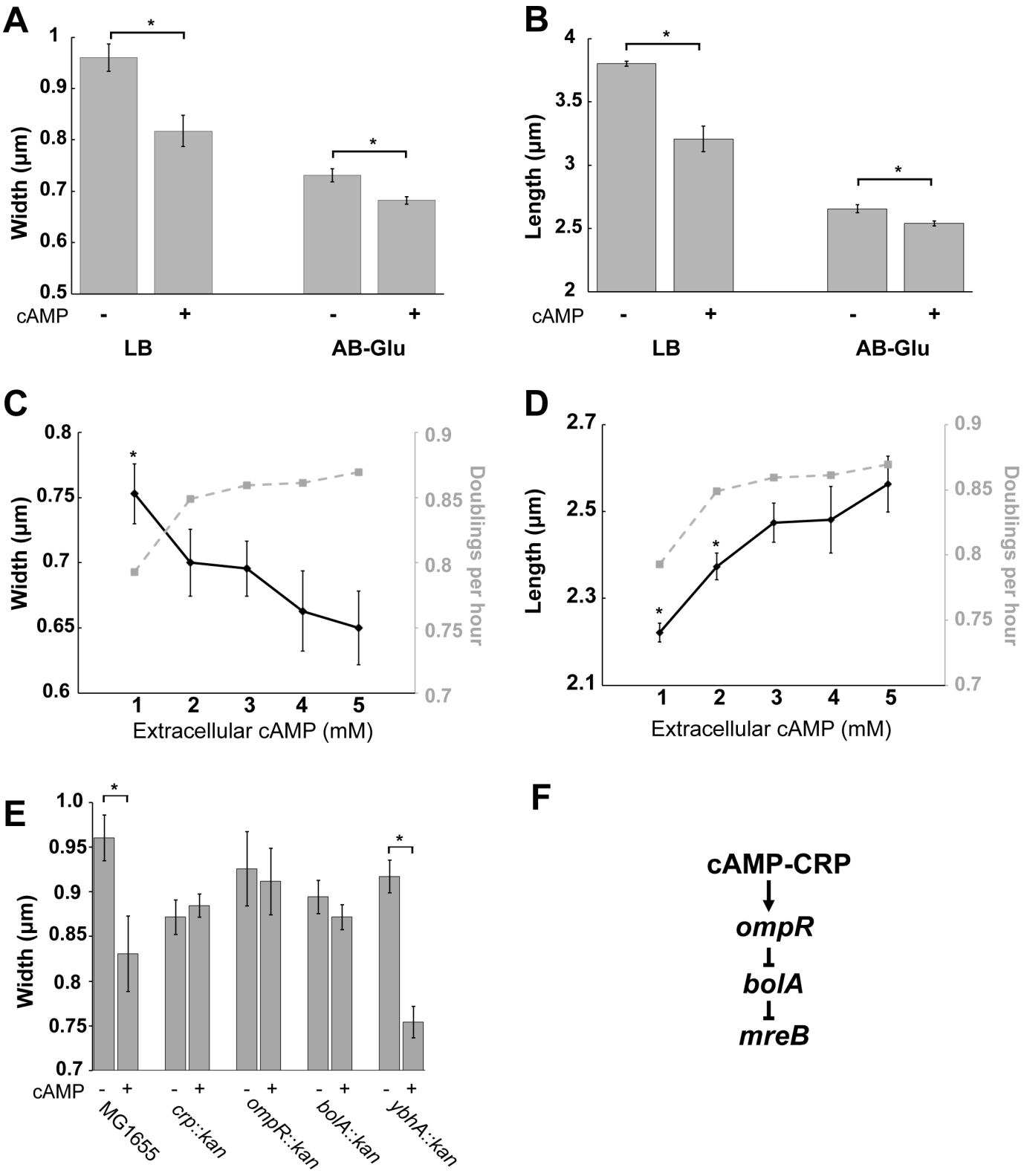

Fig 6. cAMP signaling reduces cell width via the morphogenic transcription factor *bolA*. Wild-type MG1655 cell size was measured with and without exogenous 5 mM cAMP in either LB or AB-glucose. Average width is shown in (A) and length in (B). Students' t-test was used (* p-value <. 05) to test for significance. Width (C) and length (D) of *cyaA*::*kan* grown in AB-succinate with different levels of exogenous cAMP shows that length is positively correlated with growth rate but width is not. Students' t-test was used (* p-value <. 05 compared to 5mM cAMP) to determine significance. (E) Deletions in *crp*, *ompR*, or *bolA*

abolish the cAMP-dependent cell reductions in cell width. An insertional deletion in *ybhA*, encoding a putative gluconeogenic protein, was used as a positive control. Cells were grown in LB with or without 5 mM cAMP. All points are the average of three biological replicates with a minimum of 200 cells measured per experiment. Error bars represent standard error of the mean. (F) Proposed genetic pathway linking cAMP to *mreB* transcription.

https://doi.org/10.1371/journal.pgen.1007205.g006

inhibits transcription of *mreB* [39], which encodes a key component of the elongation machinery [40]. Reductions in MreB activity lead to a block in synthesis of lateral cell wall material and the formation of wide and rounded cells [41,42]. *bolA* transcription has previously been shown to be inhibited by addition of extracellular cAMP [43].

Together, genetic interactions between *crp*, *ompR*, and *bolA*, support a model in which cAMP increases cell width indirectly, via down regulation of OmpR and the concomitant increase in BolA expression leading to repression of MreB mediated cell wall synthesis. Consistent with this model, cells defective in *ompR* and *bolA* were refractile to the addition of exogenous cAMP with regard to cell width (Fig 6E and 6F). Notably, a congenic strain encoding a deletion in *ybhA* (*ybhA*::*kan*), encoding a putative fructose-1,6-bisphosphate phosphatase [44] also exhibited cAMP-dependent reductions in growth eliminating a potential role for the *kan* cassette in this phenomenon.

Defects in acetate metabolism support links between fatty acid synthesis and assembly of the cell division machinery

Cell cycle progression is tightly correlated with growth rate in wild-type cells. Fast growing cells are not only larger but contain a higher frequency of FtsZ rings (Z-rings) with approximately 90% of *E. coli* cells containing visible Z-rings in LB-glucose. Meanwhile, slow growing cells contain fewer Z-rings (~50%). Z-ring frequency shows a roughly linear relationship to growth rate when grown in different media (Fig 4C dotted line) [13,45]. Taking advantage of a green fluorescent protein (GFP)-FtsZ fusion that allows us to label the FtsZ ring without detectably altering size or growth [6], we assessed the frequency of FtsZ ring formation in the 17 mutants in Classes I through V.

Although the Z-ring frequency and growth rate were correlated in the majority of CCM mutants, several exhibited a disconnect between these two parameters, specifically those associated with acetate metabolism and pentose phosphate pathway (black squares and green triangles respectively in Fig 4C). Cells defective in *aceE*, the E1 protein of pyruvate dehydrogenase that converts pyruvate to acetyl-CoA, exhibited an extremely high (86%) Z-ring frequency relative to wild type cells cultured in medium of the same growth rate (~75%) [13], while both *ackA* and *pta*, involved in converting acetyl-CoA to acetate, exhibited lower Z-ring frequencies relative to growth rate (69% and 67% respectively). Assembly of the cell division machinery is a multistep process involving first, recruitment of FtsZ and other so-called early proteins to the nascent division site followed by a brief delay and assembly of the late proteins, which include enzymes required for synthesis of the septal cell wall (reviewed in [46]). In *E. coli*, division is coincident with recruitment of FtsN, the last protein to be incorporated into the division machinery and the putative "trigger" for cross wall synthesis [47,48]. The two-step nature of division machinery assembly suggests two potential explanations for the elevated Z-ring frequency in *aceE*::*kan* mutants: 1) premature recruitment of FtsZ to the septum or 2) delays in late protein recruitment and activation of cytokinesis. Conversely, the lower frequency of FtsZ rings in *ackA*::*kan* and *pta*::*kan* mutants could be a consequence of either 1) delays in FtsZ recruitment or 2) premature late protein recruitment and/or activation of division mediated cell wall synthesis.

To clarify the underlying cause of the elevated Z-ring frequency in *aceE*::*kan* cells and depressed Z ring frequency in the *ackA*::*kan* and *pta*::*kan* backgrounds we took advantage of a

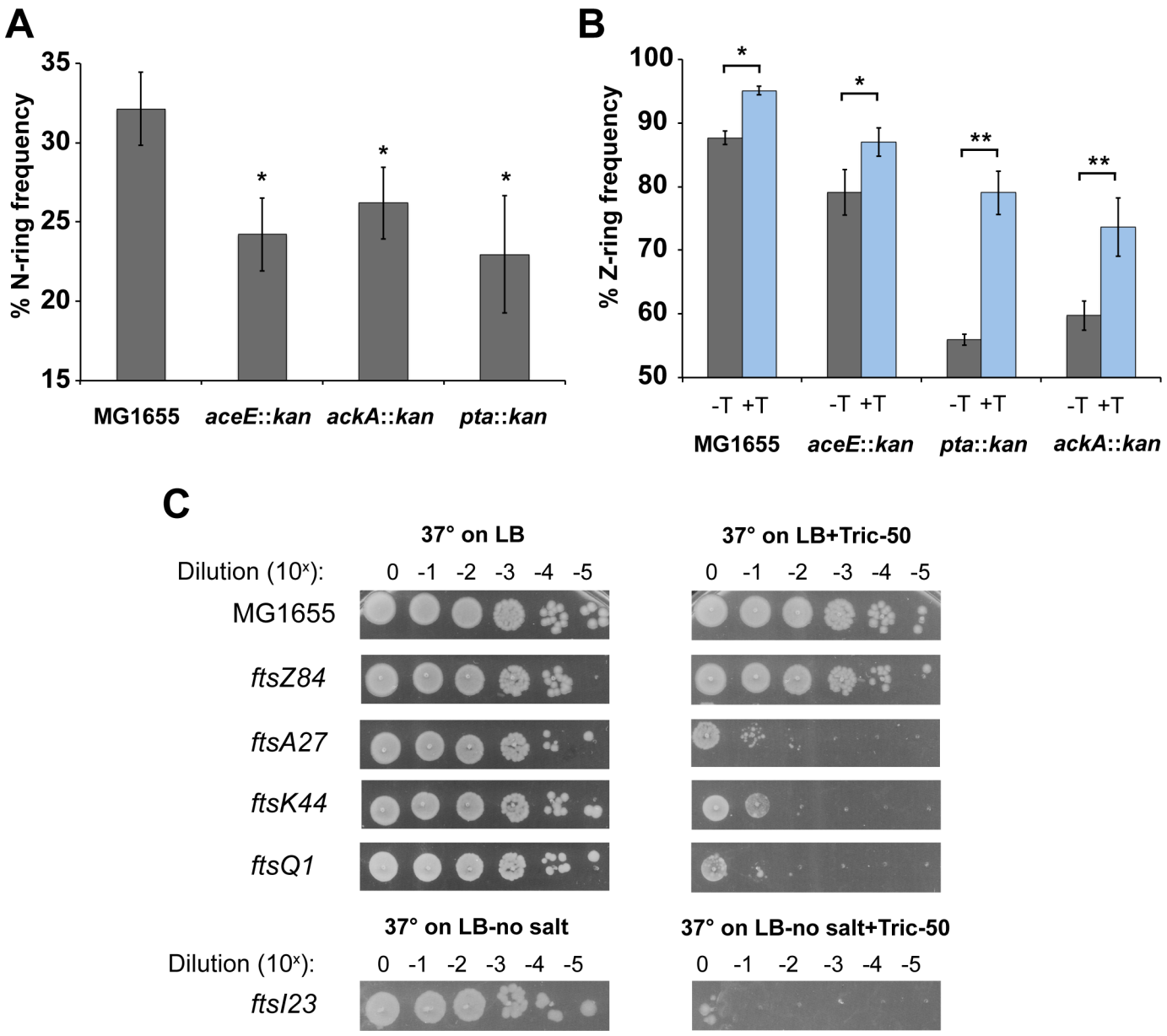

Fig 7. Partial inhibition of fatty acid synthesis negatively impacts assembly and activity of the late division proteins. (A). FtsN septal localization was measured in MG1655, *aceE*::*kan*, *ackA*::*kan*, and *pta*::*kan* expressing a chromosomal *ftsN-GFP* fusion from an IPTG inducible promoter. (B) FtsZ-ring frequency was measured for MG1655, *aceE*::*kan*, *ackA*::*kan*, and *pta*::*kan* cells expressing *ftsZ-GFP* from an IPTG-inducible promoter. Cells were cultured with (gray) or without (black) 50 ng/mL triclosan. For (A) and (B), three independent experiments were performed with a minimum of 200 cells measured per experiment. Error bars represent standard error of the mean. Significance was measured using the Students' t-test (* p-value < .05, ** p-value < .01). (C) Representative plating efficiencies of wild-type cells and the heat-sensitive cell division mutants *ftsZ84*, *ftsA27*, *ftsK44*, and *ftsQ1* cultured on LB at 37˚C with or without triclosan. *ftsI23* was plated on LB-no salt at 37˚C with or without triclosan. Plating efficiencies were repeated three times with representative images shown.

https://doi.org/10.1371/journal.pgen.1007205.g007

heterologous, IPTG-inducible FtsN-GFP [49] to assess the efficiency of FtsN recruitment in all three mutants. Growth in LB-glu showed 32% of wild-type cells with FtsN-GFP localization at mid-cell (Fig 7A). In contrast, despite varying Z-ring frequencies, all three mutants exhibit more or less the same frequency of FtsN ring formation (24%, 23%, and 26% for *aceE*::*kan*, *ackA*::*kan*, and *pta*::*kan* respectively) with all three being significantly less than wild type. The consistency of FtsN ring frequency, despite differences in Z-ring frequency between the three

CCM mutants, suggests that it is delayed recruitment of the late division proteins and/or activation of cytokinesis that is responsible for the high Z-ring frequency in *aceE*::*kan* cells while the lower Z-ring frequency in *ackA*::*kan* and *pta*::*kan* mutants would appear to be a consequence of a delay in FtsZ assembly.

Acetyl-CoA metabolism plays a critical role in the ability of cells to synthesize the wide variety of fatty acids and lipids that constitute the cell envelope [50]. *aceE*, in particular, encodes a subunit of the pyruvate dehydrogenase complex responsible for aerobic synthesis of the majority of acetyl-CoA, a necessary precursor in the first step of FAS [51]. Defects in *aceE* are thus expected to reduce flux through FAS, and based on previous work, shift the balance in lipid composition [52]. Although not directly involved in FAS, defects in *pta* and *ackA* may lead to a build-up of acetyl-CoA and potentially also shift flux through FAS.

Based on previous studies linking lipid composition to cell morphology [53], we speculated defects in acetate metabolism might result in changes in plasma membrane composition that interfere with assembly and activity of the cell division machinery. To test this idea, we measured the Z-ring frequency of wild type and mutant cells cultured in the presence of sub-inhibitory concentrations of the fatty acid synthesis inhibitor triclosan (50 ng/mL). This concentration is too low to impact growth rate but has a modest positive impact on cell size [6]. Triclosan inhibits FabI, the enzyme that catalyzes the reduction of enoyl-ACP during the elongation cycle of fatty acid synthesis [54]. Although not a perfect recapitulation of a block upstream of acetyl-CoA synthesis, as it blocks a downstream step, both triclosan treatment and the *aceE* mutations should similarly curtail flux through FAS.

In support of a model in which modest reductions in flux through FAS negatively impact assembly of the cell division machinery, Z-ring frequency was significantly increased in wild type cells as well as in *aceE*::*kan*, *pta*::*kan*, and *ackA*::*kan* cells during growth in sub-MIC (minimum inhibitory concentration), 50 ng/mL triclosan. (Z-ring frequency: wild type 88% +T/ 95% -T; *pta*::*kan* 56% -T/ 79% + T; *ackA*::*kan* 60% -T/74% +T; *aceE*::*kan* 79% -T to 87% +T) (Fig 7B). *pta* or *ackA* deletion mutants were slightly more sensitive to triclosan with regard to Z-ring frequency than either *aceE* or wild type cells, likely a reflection of the already high frequency of FtsZ rings in these latter strains.

Further supporting a connection between FAS and assembly of the cell division machinery, 50 ng/mL triclosan enhanced the heat sensitive phenotype of conditional mutations in several cell division genes including *ftsA* (*ftsA27*-an early, actin-like protein), *ftsK* (*ftsK44*—a late division protein involved in chromosome partitioning), *ftsQ* (*ftsQ1*—a late division protein believed to serve primarily as a scaffold), and *ftsI* (*ftsI23*—a late division protein with a transpeptidase domain) [55–58]. Somewhat surprisingly given its impact on FtsZ ring frequency (Fig 7B), triclosan had no impact on the heat-sensitivity of *ftsZ84* (Fig 7C). We speculate that the differential impact of triclosan on *ftsZ84* relative to the other conditional mutants is a consequence of their subcellular location (cytoplasmic–FtsZ) versus membrane associated (FtsA) and integrated into the membrane (FtsQ, FtsK, and FtsI) [46]. It is possible that these membrane associated/integral division proteins could directly sense changes in the lipid composition caused by triclosan exposure and change their activities accordingly [59]. It is also possible that fatty acid inhibition leads to changes in protein levels of known or unknown division proteins and the subcellular localization is just a coincidence.

Discussion

Our systematic analysis of the relationship between central carbon metabolism, cell growth, and cell size both reinforces the Growth Law as a general principle (i.e. growth rate and size are positively correlated) but also calls into question many of the fundamental assumptions

that underlie it. While the largest class of mutants with observable phenotypes—Class II: small with reduced growth rates, essentially "obeyed" the law so to speak, growth rate and size varied independently in the other classes of CCM mutants (Fig 1B). Class II mutants closely resemble cells cultured in nutrient-poor conditions with regard to growth rate and size, suggesting these cells are experiencing a near global reduction in biosynthetic capacity. In contrast, growth rate and morphology are independent of one another in the other nine CCM mutants (Table 1), consistent with defects in specific regulatory or structural functions that directly impact cell length and/or width.

These results are in line with accumulating work indicating that growth rate and cell size are independent phenomena. Modest defects in cell division are well known to increase bacterial cell size—particularly length—without impacting growth rate [4,7,56,57,60], while defects in transcription severely curtail growth but have little detectable impact on morphology [6]. Most importantly, exhaustive phenotypic analyses of the entirety of non-essential genes in *E. coli* in either LB or minimal glucose plus casamino acids, failed to identify any evidence supporting a direct connection between growth rate and size [16,61]. Based on recent work from the Jun lab implicating not only growth rate, but also initiation mass and cell cycle duration in the homeostatic regulation of cell size, we anticipate that further analysis of these parameters in relevant CCM mutants will provide additional insight into the specific mechanisms underlying their impact on cell morphology [10].

Although it contradicts our previous findings, our discovery that deletion of *pgm* does not suppress *ftsZ84*, as previously reported, it resolves a longstanding point of confusion. In our original study, we determined that defects in downstream genes, *galU* or *opgH*, encoding a direct inhibitor of FtsZ assembly, had little impact on *ftsZ84* cell viability. Conversely, defects in all three genes in the pathway (*pgm*, *galU*, and *opgH*), suppressed the lethality associated with overexpression of the MinD division inhibitor. We anticipate this discrepancy in suppression ability is related to the mechanism underlying *ftsZ84* heat sensitivity and *MinD* interference in FtsZ assembly. While the former is a consequence of mutations in the GTP binding site that dramatically impair nucleotide binding and subunit-subunit interactions, the latter impacts FtsZ assembly in a GTP independent manner [7,62,63].

Nutrient limitation abrogates defects in CCM mutant morphology

The similarity between wild-type and CCM mutant cell size during growth in nutrient rich medium almost certainly reflects reductions in metabolic flux that impact wild type cells to a greater degree than their CCM defective counterparts. While CCM mutants are forced to use alternative, less efficient pathways to maximize growth in rich medium, limiting quantities of key nutrients in poor medium level the playing field, requiring wild type cells to similarly redirect key aspects of anabolic metabolism. For example, acetate mutants (*aceE*, *ackA*, *pta*) are unable to fully utilize carbon during growth in nutrient rich medium due to a block in overflow metabolism, while during growth in AB-glucose, both acetate mutants and wild type cells are more able to fully oxidize glucose and are not limited by the need to excrete acetate. In other cases, growth in nutrient poor medium may ameliorate the accumulation of metabolites that function indirectly to inhibit growth. *zwf*::*kan* and *tpiA*::*kan* mutants most likely fall into this group. The zwf protein product, glucose-6-phosphate dehydrogenase, is required for synthesis of a large portion of cellular NADPH, a key factor in glutathione recycling. Glutathione in turn, is essential for neutralizing reactive oxygen species (ROS), which are generated at high levels during growth in nutrient rich conditions [64]. *zwf* mutants, including *zwf*::*kan*, are hypersensitive to oxidizing agents during growth in nutrient rich medium [65]. This hypersensitivity is absent during growth in nutrient poor medium due to the reduction in ROS,

allowing cells to recycle glutathione through other pathways. Likewise, deletion of *tpiA* leads to over-accumulation of dihydroxyacetone, which can be converted into pyruvate through the methylglyoxate pathway. During growth in nutrient rich medium, high rates of flux through this pathway result in accumulation of the toxic compound, methylglyoxate, which methylates DNA [66]. Reduced metabolic flux in nutrient poor medium could allow removal of dihydroxyacetone without methylglyoxate accumulation.

Overflow metabolism and cell size

In a common, yet paradoxical, fermentative mechanism known as "overflow metabolism", *E. coli* convert up to 50% of available glucose into acetate during aerobic growth in nutrient rich conditions [67]. Acetate fermentation is inefficient, resulting in ~14 fewer ATP per glucose than oxidative phosphorylation and, unlike other fermentative pathways, does not regenerate NAD^+ from NADH [24]. While it is unclear why bacteria perform overflow metabolism, it is potentially a more proteome-efficient means of moving carbon through CCM, ensuring that glycolysis proceeds at a maximum pace when nutrients are plentiful.

Supporting the idea that overflow metabolism is critical for maximizing glycolytic flux, defects in *pta*, *ackA*, and *aceE*, encoding the first two enzymes in acetate fermentation and a subunit of pyruvate dehydrogenase respectively, are dramatically impaired in both growth rate and cell size. This is consistent with a global reduction in biosynthetic capacity. Whether this reduction is the result of lower ATP production or the consequence of a bottleneck in flux through critical biosynthetic pathways is unclear. Regardless, we suspect that reductions in ATP levels and/or biosynthesis indirectly result in accumulation of the alarmone ppGpp [68], providing an explanation for the observed suppression of *ftsZ84* heat-sensitivity in *pta*, *ackA*, and *aceE* deletion strains. Increases in ppGpp are well known to suppress the conditional nature of *ftsZ84*, although the precise mechanism has yet to be determined [20,69].

cAMP is a key player in maintaining the correct cellular aspect ratio

A somewhat surprising finding is the identification of cAMP as a contributor to nutrient dependent reduction in both cell length and width. Accumulating under gluconeogenic conditions, cAMP binds to the transcriptional activator Crp and regulates expression of more the than 280 genes [70]. Although the member(s) of the cAMP-Crp regulon responsible remains elusive, our data indicate that cAMP-Crp reduce width under nutrient poor conditions via their impact on the morphogenic factor BolA and cell length via their impact on FtsZ assembly (Figs 5 and 6).

In this regard, cAMP differs from metabolic signaling molecule, ppGpp, which genetics indicate is a positive regulator of division (Fig 8). Increases in ppGpp reduce cell length and

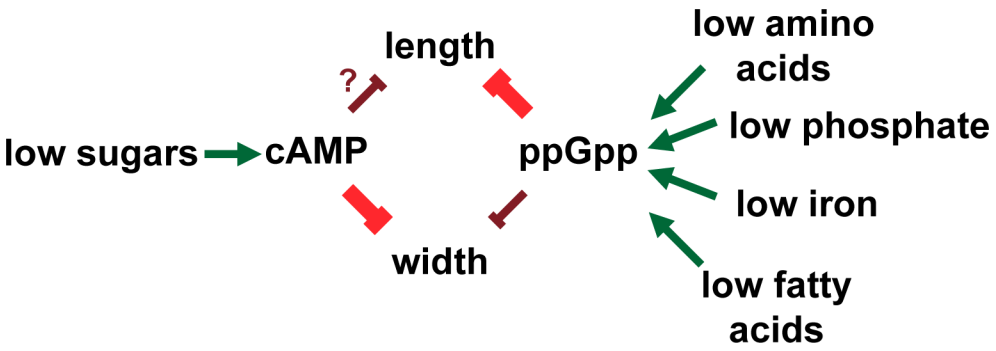

Fig 8. Proposed pathway linking nutrient levels to cell length and width through the signaling nucleotides cAMP and ppGpp.

https://doi.org/10.1371/journal.pgen.1007205.g008

suppress *ftsZ84* heat sensitivity, while deletion of both ppGpp synthetatases, *relA* and *spoT*, increase cell length and enhance *ftsZ84* heat sensitivity [6,20]. In contrast, the effect of cAMP on cell morphology is less clear-cut. In an apparent contradiction, both the loss of cAMP signaling and the addition exogenous cAMP, lead to reductions in cell length (Table 1 and Fig 6). cAMP signaling controls a large number of genes required for different types of carbon assimilation. The contradictory nature of our cAMP data likely reflects differences in the ability of cells to utilize different carbon sources in complex medium, altering biosynthetic capacity and elongation rates in unpredictable ways.

CCM is robust but not necessarily efficient

Perhaps the biggest surprise of this study is our finding that the defects in the majority of non-essential CCM genes had little to no detectable impact on either cell size or growth rate. While the lack of phenotype in many cases is likely a consequence of our screening conditions, nutrient-rich, complex medium supplemented with glucose, in certain cases the robust growth we observed is difficult to explain. For example, we anticipated that defects in phosphoglucose isomerase (encoded by *pgi*), the first dedicated step in glycolysis would dramatically impact growth rate and size by virtue of its impact on not only glycolysis, but also other associated pathways leading to reductions in ATP synthesis and overall biosynthetic capacity [71]. Instead, we were unable to distinguish *pgi* mutants from wild type cells during growth LB-glucose (S2 Table). Based on our identification of seven mutants in the pentose-phosphate pathway, we hypothesize that despite the ubiquitous nature of glycolysis in nutrient- rich medium, glucose is predominantly driven through the pentose-phosphate pathway to generate essential building blocks.

Similarly, we observed little in the way of a detectable phenotype associated with defects in the gene encoding citrate synthase *gltA*. Essential for the complete oxidation of carbon, GltA synthesizes citrate from oxaloacetate and acetyl-CoA at the entry point into the TCA cycle [72]. Despite its seeming importance, previous work indicates that *E. coli* represses *gltA* transcription in the presence of glucose, suggesting that it can forgo complete carbon oxidation under nutrient rich conditions [70,73]. It may be that under nutrient rich condition, *E. coli* maximizes rapid growth over the efficient use of available carbon, a proposition that is in line with our data indicating that defects in acetate metabolism significantly curtail growth in nutrient rich medium (Table 1).

Concluding thoughts

While this screen demonstrates the ability of systematic phenotypic analysis to identify new connections between CCM, cell growth and cell size, many questions remain unanswered. In addition to the large number of insertion mutants with no observable phenotype, defects in 17 genes resulted in dramatic changes in growth rate and cell morphology. Of these, we were able to identify the proximal cause in 24% (*crr*, *aceE*, *pta*, *ackA*; Figs 5–7). A better understanding of the remaining 13 mutations will likely require a combination of genetics and metabolomics to tease apart the root cause of their morphological and growth related defects.

Additionally, although this effort focused specifically on carbon metabolism, the availability of other nutrients—particularly nitrogen, phosphorous, sulfur and iron—have also been implicated in growth and morphology. Assessing the phenotype of the CCM insertion collection under conditions in which these factors are limiting is thus also worthwhile. Finally, *E. coli* is believed to spend much of its time under microaerobic or anaerobic conditions. Understanding how oxygen levels impact growth, cell cycle progression, and cell morphology thus remains a tantalizingly open question.

Materials and methods

Strains and media

All chemicals, media components, and antibiotics were purchased from Sigma-Aldrich (St. Louis, MO). *E. coli* strains were constructed through standard P1 vir transductions [74] moving kanamycin marked insertion deletions from Keio collection strains [21] purchased from the Coli Genomic Stock Center into MG1655 (F^- λ^- *ilvG- rfb*-50 *rph*-1), our "wild type" parental strain. Cell were cultured in Luria-Bertani (LB) broth supplemented with 0.2% glucose or AB defined media [75] supplemented with either 0.2% glucose or 0.2% succinate as the sole carbon source. Unless otherwise noted (e.g. for heat sensitive conditional alleles of cell division genes including *ftsZ84*, *ftsA27*, *ftsK44*, *ftsQ1*, and *ftsI23*), cells were cultured at 37˚ C and sampled for analysis at OD_{600} between 0.1 and 0.2. For the primary analysis cells were cultured in 5 mL LB + 0.2% glucose and aerated at 200 rpm. For measuring the effect of different media, cells were cultured in 200 μL of specified media in a 96-well plate and aerated at 567 rpm in a BioTek Eon plate reader (Fig 3).

Microscopy

Cells were sampled directly from cultures and fixed in 16% paraformaldehyde (Electron Microscopy Sciences) as described [6]. Fixed cells were mounted on agarose pads and visualized using a 100x phase-fluor objective on a Nikon Ti-E inverted microscope. To facilitate visualization of FtsZ rings, 1 mM IPTG was added to cultures of cells encoding a chromosomal P_{IPTG}-*ftsZ-GFP* [76]. Expression of a chromosomal P_{IPTG}-*ftsN-GFP* was induced with 50 μM IPTG [49]. GFP fluorescence was detected with a C-FL GFP filter cube with 470/40nm excitation and 525/50nm emission (Chroma Technology Corporation) Nikon Elements software (Nikon Instruments, Inc.) was used for image capture and analysis. >200 cells were counted per experimental replicate and at least three independent replicates were used for each data point.

Cell size measurements

Cell size from phase-contrast images was determined with one of two freely available segmentation software packages: the ImageJ plug-in Coli Inspector [22] (Fig 1, Table 1, and S2 Table) or SuperSegger, a MatLab based application [23] (Figs 3–7, S3 Table). As Coli Inspector does not determine area directly, we estimated it as length x width. SuperSegger directly determines the area of individual cells. We determined the area of ≥200 cells for each experiment and/or condition. Unless otherwise noted, average size was determined from 3 independent experiments.

Dot plating efficiency assays

Heat-sensitive cell division alleles, *ftsZ84*, *ftsA27*, *ftsK44*, *ftsQ1*, and *ftsI23* were cultured in LB at 30˚C degrees to an OD_{600} of ~0.5. 1 mL of cells were then pelleted, washed once with LB-no salt, and re-suspended to an OD_{600} of 0.1 in LB-no salt. 10 μL of serial dilutions between 10^{-1} to 10^{-6} were plated under permissive conditions (LB at 30˚C) or non-permissive conditions (LB-no salt at 37˚C). Due to the strains extreme sensitivity, LB-no salt at 30˚C was non-permissive for *zwf*::*kan ftsZ84* double mutants. For cAMP or triclosan addition experiments, 5 mM cAMP or 50 ng/mL triclosan was added directly to LB agar prior to pouring the plates. Each plating efficiency experiment was repeated three times with representative images shown.

Supporting information

S1 Table. List of bacterial strains used in this study.
(DOCX)

S2 Table. Raw size and growth rate data for all central carbon metabolic gene deletions.
(XLSX)

S3 Table. Raw data for Fig 3 (CCM mutant growth in different media).
(XLSX)

S4 Table. Raw data for Fig 4C (Z-ring frequency of CCM mutants).
(XLSX)

S1 Fig. Relationship between aspect ratio (length/width) and growth rate. Length and width data from Table 1 were used to generate the aspect ratio for each CCM mutant (blue triangles). Aspect ratio data for different media was generated from S3 Table (black squares) or from previously reported results (orange diamond) [6].
(TIF)

S2 Fig. The effect of cell fixation on cell size. MG1655 and *aceE*::*kan* cells were grown in LB-glu and were either directly measured (unfixed) or fixed with paraformaldehyde-glutaraldehyde then measured. Average cell length (A), width (B), or area (C) are shown. Data is from three independent experiments with >200 cells measured per experiment. Error bars represent the standard error of the mean.
(TIF)

S3 Fig. Histograms of cell length data for the short and long mutants. Length data of 1000 cells from the LB-glu growth condition from S3 Table was binned into 0.5 μm bins for MG1655 (black line), *zwf*::*kan* (orange dash-dot) and *acnB*::*kan* (blue dots).
(TIF)

S4 Fig. Nutrient dependent effects on cell length for CCM mutants. Average length data for the CCM mutants grown in LB-glu, AB-glu, and AB-suc divided into Entner-Doudoroff, gluconeogenesis, and TCA (A), pentose phosphate pathway (B), acetate fermentation (C), cAMP synthesis (D). Error bars represent standard error of the mean. Data is from three independent experiments with >200 cells measured per experiment. N.G. indicates no growth in the condition shown.
(TIF)

S5 Fig. Nutrient dependent effects on cell width for CCM mutants. Average width data for the CCM mutants in LB-glu, AB-glu, and AB-suc divided into Entner-Doudoroff, gluconeogenesis, and TCA (A), pentose phosphate pathway (B), and acetate fermentation (C). cAMP mutants are shown in Fig 3E. Wild-type MG1655 data is shown in each panel to aid in comparison. Error bars represent standard error of the mean. Data is from three independent experiments with >200 cells measured per experiment. N.G. indicates no growth in condition shown.
(TIF)

Acknowledgments

We would like to thank the Coli Genetic Stock Center (CGSC) for providing numerous strains quickly. We'd like to thank Norbert Vischer for aid in using Coli Inspector and Stella Stylianidou and Paul Wiggins for help with SuperSegger. We would like to thank Elizabeth Mueller

for work on the *pgm ftsZ84* double mutant. We would also like to thank Elizabeth Mueller, Dr. Ashley Sherp, and the Hani Zaher laboratory for critical feedback on this work.

Author Contributions

Conceptualization: Corey S. Westfall, Petra Anne Levin.

Formal analysis: Petra Anne Levin.

Investigation: Corey S. Westfall.

Methodology: Corey S. Westfall, Petra Anne Levin.

Writing – original draft: Corey S. Westfall, Petra Anne Levin.

Writing – review & editing: Corey S. Westfall, Petra Anne Levin.

References

1. Schaechter M, Maaløe O, Kjeldgaard NO. Dependency on medium and temperature of cell size and chemical composition during balanced grown of Salmonella typhimurium. J Gen Microbiol. 1958; 19: 592–606. https://doi.org/10.1099/00221287-19-3-592 PMID: 13611202
2. Sargent MG. Control of cell length in Bacillus subtilis. J Bacteriol. 1975; 123: 7–19. PMID: 806582
3. Donachie WD, Begg KJ. Cell length, nucleoid separation, and cell division of rod-shaped and spherical cells of Eschericia coli. J Bacteriol. 1989; 171: 4633–4639. PMID: 2670889
4. Weart RB, Lee AH, Chien A-C, Haeusser DP, Hill NS, Levin PA. A metabolic sensor governing cell size in bacteria. Cell. 2007; 130: 335–347. https://doi.org/10.1016/j.cell.2007.05.043 PMID: 17662947
5. Donachie WD. Relationship between cell size and time of initiation of DNA replication. Nature. 1968; 219: 1077–9. PMID: 4876941
6. Vadia S, Jessica LT, Lucena R, Yang Z, Kellogg DR, Wang JD, et al. Fatty Acid Availability Sets Cell Envelope Capacity and Dictates Microbial Cell Size. Current Biology. 2017.
7. Arjes HA, Lai B, Emelue E, Steinbach A, Levin PA. Mutations in the bacterial cell division protein FtsZ highlight the role of GTP binding and longitudinal subunit interactions in assembly and function. BMC Microbiol. 2015; 15: 209. https://doi.org/10.1186/s12866-015-0544-z PMID: 26463348
8. Coltharp C, Buss J, Plumer TM, Xiao J. Defining the rate-limiting processes of bacterial cytokinesis. Proc Natl Acad Sci USA. 2016; 113: E1044–53. https://doi.org/10.1073/pnas.1514296113 PMID: 26831086
9. Zheng H, Ho P-Y, Jiang M, Tang Bin, Liu W, Li D, et al. Interrogating the Escherichia coli cell cycle by cell dimension perturbations. P Natl Acad Sci USA. 2016; 113: 15000–15005.
10. Si F, Li D, Cox SE, Sauls JT, Azizi O, Sou C, et al. Invariance of Initiation Mass and Predictability of Cell Size in Escherichia coli. Curr Biol. 2017; 27: 1278–1287. https://doi.org/10.1016/j.cub.2017.03.022 PMID: 28416114
11. Tymecka-Mulik J, Boss L, Maciąg-Dorszyńska M, Rodrigues JFM, Gaffke L, Wosinski A, et al. Suppression of the Escherichia coli dnaA46 mutation by changes in the activities of the pyruvate-acetate node links DNA replication regulation to central carbon metabolism. Korolev S, editor. PLoS ONE. Public Library of Science; 2017; 12: e0176050. https://doi.org/10.1371/journal.pone.0176050 PMID: 28448512
12. Monahan LG, Hajduk IV, Blaber SP, Charles IG, Harry EJ. Coordinating bacterial cell division with nutrient availability: a role for glycolysis. MBio. 2014; 5. https://doi.org/10.1128/mBio.00935-14 PMID: 24825009
13. Hill NS, Buske PJ, Shi Y, Levin PA. A Moonlighting Enzyme Links Escherichia coli Cell Size with Central Metabolism. PLoS Genet. Public Library of Science; 2013; 9: e1003663. https://doi.org/10.1371/journal.pgen.1003663 PMID: 23935518
14. Irnov I, Wang Z, Jannetty ND, Bustamante JA, Rhee KY, Jacobs-Wagner C. Crosstalk between the tricarboxylic acid cycle and peptidoglycan synthesis in Caulobacter crescentus through the homeostatic control of α-ketoglutarate. Casadesús J, editor. PLoS Genet. Public Library of Science; 2017; 13: e1006978. https://doi.org/10.1371/journal.pgen.1006978 PMID: 28827812
15. French S, Côté J-P, Stokes JM, Truant R, Brown ED. Bacteria Getting into Shape: Genetic Determinants of E. coli Morphology. Dunman P, editor. MBio. American Society for Microbiology; 2017; 8: e01977–16. https://doi.org/10.1128/mBio.01977-16 PMID: 28270582

16. Campos M, Dobihal GS, Jacobs-Wagner C. Genome-wide phenotypic analysis of growth, cell morphogenesis and cell cycle events in Escherichia coli. bioRxiv. Cold Spring Harbor Labs Journals; 2017;: 101832. https://doi.org/10.1101/101832
17. Yao Z, Davis RM, Kishony R, Kahne D, Ruiz N. Regulation of cell size in response to nutrient availability by fatty acid biosynthesis in Escherichia coli. Proc Natl Acad Sci USA. 2012; 109: E2561–8. https://doi.org/10.1073/pnas.1209742109 PMID: 22908292
18. Jorgenson MA, Kannan S, Laubacher ME, Young KD. Dead-end intermediates in the enterobacterial common antigen pathway induce morphological defects in Escherichia coli by competing for undecaprenyl phosphate. Mol Microbiol. 2015; 100: 1–14. https://doi.org/10.1111/mmi.13284 PMID: 26593043
19. Magnusson LU, Farewell A, Nyström T. ppGpp: a global regulator in Escherichia coli. Trends in Microbiology. 2005.
20. Powell BS, Court DL. Control of ftsZ expression, cell division, and glutamine metabolism in Luria-Bertani medium by the alarmone ppGpp in Escherichia coli. J Bacteriol. 1998; 180: 1053–1062. PMID: 9495742
21. Baba T, Ara T, Hasegawa M, Takai Y, Okumura Y, Baba M, et al. Construction of Escherichia coli K-12 in-frame, single-gene knockout mutants: the Keio collection. Mol Syst Biol. EMBO Press; 2006; 2: 2006.0008. https://doi.org/10.1038/msb4100050 PMID: 16738554
22. Vischer NOE, Verheul J, Postma M, van den Berg van Saparoea B, Galli E, Natale P, et al. Cell age dependent concentration of Escherichia coli divisome proteins analyzed with ImageJ and ObjectJ. Front Microbiol. 2015; 6: 586. https://doi.org/10.3389/fmicb.2015.00586 PMID: 26124755
23. Stylianidou S, Brennan C, Nissen SB, Kuwada NJ, Wiggins PA. SuperSegger: robust image segmentation, analysis and lineage tracking of bacterial cells. Mol Microbiol. 2016; 102: 690–700. https://doi.org/10.1111/mmi.13486 PMID: 27569113
24. Basan M, Hui S, Okano H, Zhang Z, Shen Y. Overflow metabolism in Escherichia coli results from efficient proteome allocation. Nature. Nature Publishing Group; 2015; 528: 99–104. https://doi.org/10.1038/nature15765 PMID: 26632588
25. Joyce AR, Reed JL, White A, Edwards R, Osterman A, Baba T, et al. Experimental and computational assessment of conditionally essential genes in Escherichia coli. J Bacteriol. American Society for Microbiology; 2006; 188: 8259–8271. https://doi.org/10.1128/JB.00740-06 PMID: 17012394
26. Alwine JC, Russell RM, Murray KN. Characterization of an Escherichia coli mutant deficient in dihydrolipoyl dehydrogenase activity. J Bacteriol. American Society for Microbiology (ASM); 1973; 115: 1–8. PMID: 4197899
27. Gabor E, Göhler A-K, Kosfeld A, Staab A, Kremling A, Jahreis K. The phosphoenolpyruvate-dependent glucose-phosphotransferase system from Escherichia coli K-12 as the center of a network regulating carbohydrate flux in the cell. Eur J Cell Biol. 2011; 90: 711–720. https://doi.org/10.1016/j.ejcb.2011.04.002 PMID: 21621292
28. Deutscher J, Francke C, Postma PW. How phosphotransferase system-related protein phosphorylation regulates carbohydrate metabolism in bacteria. Microbiol Mol Biol Rev. American Society for Microbiology; 2006; 70: 939–1031. https://doi.org/10.1128/MMBR.00024-06 PMID: 17158705
29. Saier MH, Feucht BU, Hofstadter LJ. Regulation of carbohydrate uptake and adenylate cyclase activity mediated by the enzymes II of the phosphoenolpyruvate: sugar phosphotransferase system in Escherichia coli. J Biol Chem. American Society for Biochemistry and Molecular Biology; 1976; 251: 883–892. PMID: 765335
30. Park Y-H, Lee BR, Seok Y-J, Peterkofsky A. In vitro reconstitution of catabolite repression in Escherichia coli. J Biol Chem. American Society for Biochemistry and Molecular Biology; 2006; 281: 6448–6454. https://doi.org/10.1074/jbc.M512672200 PMID: 16407219
31. Zubay G, Schwartz D, Beckwith J. Mechanism of activation of catabolite-sensitive genes: a positive control system. P Natl Acad Sci USA. National Academy of Sciences; 1970; 66: 104–110.
32. Grainger DC, Hurd D, Harrison M, Holdstock J, Busby SJW. Studies of the distribution of Escherichia coli cAMP-receptor protein and RNA polymerase along the E. coli chromosome. P Natl Acad Sci USA. National Acad Sciences; 2005; 102: 17693–17698. https://doi.org/10.1073/pnas.0506687102 PMID: 16301522
33. Ricard M, Hirota Y. Process of cellular division in Escherichia coli: physiological study on thermosensitive mutants defective in cell division. J Bacteriol. 1973; 116: 314–322. PMID: 4583216
34. Addinall SG, Lutkenhaus CJ. Temperature shift experiments with anftsZ84(Ts) strain reveal rapid dynamics of FtsZ localization and indicate that the Z ring is required throughout septation and cannot reoccupy division sites once constriction has initiated. J Bacteriol. 1997; 179: 4277–4284. PMID: 9209044
35. Levin PA, Kurtser IG, Grossman AD. Identification and characterization of a negative regulator of FtsZ ring formation in Bacillus subtilis. P Natl Acad Sci USA. 1999; 96: 9642–9647.

36. Gervais FG, Drapeau GR. Identification, cloning, and characterization of rcsF, a new regulator gene for exopolysaccharide synthesis that suppresses the division mutation ftsZ84 in Escherichia coli K-12. J Bacteriol. 1992; 174: 8016–8022. PMID: 1459951

37. Jackson DW, Simecka JW, Romeo T. Catabolite repression of Escherichia coli biofilm formation. J Bacteriol. American Society for Microbiology (ASM); 2002; 184: 3406–3410. https://doi.org/10.1128/JB.184.12.3406-3410.2002 PMID: 12029060

38. Huang L, Tsui P, Freundlich M. Positive and negative control of ompB transcription in Escherichia coli by cyclic AMP and the cyclic AMP receptor protein. J Bacteriol. American Society for Microbiology (ASM); 1992; 174: 664–670. PMID: 1310090

39. Yamamoto K, Nagura R, Tanabe H, Fujita N, Ishihama A, Utsumi R. Negative regulation of the bolA1p of Escherichia coli K-12 by the transcription factor OmpR for osmolarity response genes. FEMS Microbiol Lett. 2000; 186: 257–262. PMID: 10802181

40. Doi M, Wachi M, Ishino F, Tomioka S, Ito M, Sakagami Y, et al. Determinations of the DNA sequence of the mreB gene and of the gene products of the mre region that function in formation of the rod shape of Escherichia coli cells. J Bacteriol. American Society for Microbiology; 1988; 170: 4619–4624. https://doi.org/10.1128/jb.170.10.4619–4624.1988 PMID: 3049542

41. Kruse T, Bork-Jensen J, Gerdes K. The morphogenetic MreBCD proteins of Escherichia coli form an essential membrane-bound complex. Mol Microbiol. Blackwell Publishing Ltd; 2005; 55: 78–89. https://doi.org/10.1111/j.1365-2958.2004.04367.x PMID: 15612918

42. Divakaruni AV, Baida C, White CL, Gober JW. The cell shape proteins MreB and MreC control cell morphogenesis by positioning cell wall synthetic complexes. Mol Microbiol. 2007 ed. 2007; 66: 174–188. https://doi.org/10.1111/j.1365-2958.2007.05910.x PMID: 17880425

43. Lange R, Hengge-Aronis R. Growth phase-regulated expression of bolA and morphology of stationary-phase Escherichia coli cells are controlled by the novel sigma factor sigma S. J Bacteriol. 1991; 173: 4474–4481. PMID: 1648559

44. Kuznetsova E, Proudfoot M, Gonzalez CF, Brown G, Omelchenko MV, Borozan I, et al. Genome-wide analysis of substrate specificities of the Escherichia coli haloacid dehalogenase-like phosphatase family. J Biol Chem. American Society for Biochemistry and Molecular Biology; 2006; 281: 36149–36161. https://doi.org/10.1074/jbc.M605449200 PMID: 16990279

45. Weart RB, Levin PA. Growth rate-dependent regulation of medial FtsZ ring formation. J Bacteriol. 2003; 185: 2826–2834. https://doi.org/10.1128/JB.185.9.2826-2834.2003 PMID: 12700262

46. Margolin W. FtsZ and the division of prokaryotic cells and organelles. Nat Rev Mol Cell Biol. 2005; 6: 862–871. https://doi.org/10.1038/nrm1745 PMID: 16227976

47. Lutkenhaus J. FtsN—trigger for septation. J Bacteriol. 2009; 191: 7381–7382. https://doi.org/10.1128/JB.01100-09 PMID: 19854895

48. Daley DO, Skoglund U, Söderström B. FtsZ does not initiate membrane constriction at the onset of division. Sci Rep. 2016; 6: 33138. https://doi.org/10.1038/srep33138 PMID: 27609565

49. Gerding MA, Liu B, Bendezú FO, Hale CA, Bernhardt TG, de Boer PAJ. Self-enhanced accumulation of FtsN at Division Sites and Roles for Other Proteins with a SPOR domain (DamX, DedD, and RlpA) in Escherichia coli cell constriction. J Bacteriol. 2009; 191: 7383–7401. https://doi.org/10.1128/JB.00811-09 PMID: 19684127

50. Parsons JB, Rock CO. Bacterial lipids: Metabolism and membrane homeostasis. Progress in Lipid Research. 2013; 52: 249–276. https://doi.org/10.1016/j.plipres.2013.02.002 PMID: 23500459

51. Li M, Ho PY, Yao S, Shimizu K. Effect of lpdA gene knockout on the metabolism in Escherichia coli based on enzyme activities, intracellular metabolite concentrations and metabolic flux analysis by . . .. Journal of biotechnology. 2006.

52. Buttke TM, Ingram L. Inhibition of unsaturated fatty acid synthesis in Escherichia coli by the antibiotic cerulenin. Biochemistry. 1978.

53. Rowlett VW, Mallampalli VKPS, Karlstaedt A, Dowhan W, Taegtmeyer H, Margolin W, et al. Impact of Membrane Phospholipid Alterations in Escherichia coli on Cellular Function and Bacterial Stress Adaptation. jbasmorg.

54. McMurry LM, Oethinger M, Levy SB. Triclosan targets lipid synthesis. Nature. 1998; 394: 531–532. https://doi.org/10.1038/28970 PMID: 9707111

55. Herricks JR, Nguyen D, Margolin W. A thermosensitive defect in the ATP binding pocket of FtsA can be suppressed by allosteric changes in the dimer interface. Mol Microbiol. 2014; 94: 713–727. https://doi.org/10.1111/mmi.12790 PMID: 25213228

56. Begg KJ, Dewar SJ, Donachie WD. A new Escherichia coli cell division gene, ftsK. J Bacteriol. American Society for Microbiology; 1995; 177: 6211–6222. https://doi.org/10.1128/jb.177.21.6211–6222.1995 PMID: 7592387

57. Storts DR, Aparicio OM, Schoemaker JM, Markovitz A. Overproduction and identification of the ftsQ gene product, an essential cell division protein in Escherichia coli K-12. J Bacteriol. American Society for Microbiology (ASM); 1989; 171: 4290–4297. PMID: 2546918

58. Begg KJ, Donachie WD. Cell shape and division in Escherichia coli: experiments with shape and division mutants. J Bacteriol. 1985; 163: 615–622. PMID: 3894330

59. Mileykovskaya E, Sun Q, Margolin W, Dowhan W. Localization and Function of Early Cell Division Proteins in Filamentous Escherichia coli Cells Lacking Phosphatidylethanolamine. Journal of . . .. 1998.

60. Labie C, Bouche F, Bouche JP. Isolation and mapping of Escherichia coli mutations conferring resistance to division inhibition protein DicB. J Bacteriol. 1989; 171: 4315–4319. PMID: 2666395

61. Ursell T, Lee TK, Shiomi D, Shi H, Tropini C, Monds RD, et al. Rapid, precise quantification of bacterial cellular dimensions across a genomic-scale knockout library. BMC Biol. BioMed Central; 2017; 15: 17. https://doi.org/10.1186/s12915-017-0348-8 PMID: 28222723

62. RayChaudhuri D, Park JT. Escherichia colicell-division geneftsZencodes a novel GTP-binding protein. Nature. 1992; 259: 251–254.

63. de Boer PAJ, Crossley RE, Rothfield LI. Roles of MinC and MinD in the site-specific septation block mediated by the MinCDE system ofEscherichia coli. J Bacteriol. 1992; 174: 63–70. PMID: 1729224

64. Imlay JA. Cellular defenses against superoxide and hydrogen peroxide. Annu Rev Biochem. Annual Reviews; 2008; 77: 755–776. https://doi.org/10.1146/annurev.biochem.77.061606.161055 PMID: 18173371

65. Sandoval JM, Arenas FA, Vásquez CC. Glucose-6-phosphate dehydrogenase protects Escherichia coli from tellurite-mediated oxidative stress. Appanna VD, editor. PLoS ONE. 2011; 6: e25573. https://doi.org/10.1371/journal.pone.0025573 PMID: 21984934

66. Paterson GK, Cone DB, Northen H, Peters SE, Maskell DJ. Deletion of the gene encoding the glycolytic enzyme triosephosphate isomerase (tpi) alters morphology of Salmonella enterica serovar Typhimurium and decreases fitness in mice. FEMS Microbiol Lett. 2009; 294: 45–51. https://doi.org/10.1111/j.1574-6968.2009.01553.x PMID: 19493007

67. Aristidou AA, San KY, Bennett GN. Metabolic engineering of Escherichia coli to enhance recombinant protein production through acetate reduction. Biotechnol Prog. American Chemical Society; 1995; 11: 475–478. https://doi.org/10.1021/bp00034a019 PMID: 7654314

68. Liu K, Bittner AN, Wang JD. Diversity in (p)ppGpp metabolism and effectors. Curr Opin Microbiol. 2015; 24C: 72–79. https://doi.org/10.1016/j.mib.2015.01.012 PMID: 25636134

69. Navarro F, Robin A, D'Ari R, Joseleau-Petit D. Analysis of the effect of ppGpp on the ftsQAZ operon in Escherichia coli. Mol Microbiol. 1998; 29: 815–823. PMID: 9723920

70. Zheng D, Constantinidou C, Hobman JL, Minchin SD. Identification of the CRP regulon using in vitro and in vivo transcriptional profiling. Nucleic Acids Res. 2004; 32: 5874–5893. https://doi.org/10.1093/nar/gkh908 PMID: 15520470

71. Adhya S, Schwartz M. Phosphoglucomutase mutants of Escherichia coli K-12. J Bacteriol. 1971; 108: 621–626. PMID: 4942754

72. Spencer ME, Guest JR. Molecular cloning of four tricarboxylic acid cyclic genes of Escherichia coli. J Bacteriol. American Society for Microbiology (ASM); 1982; 151: 542–552. PMID: 6284701

73. Walsh K, Koshland DE. Characterization of rate-controlling steps in vivo by use of an adjustable expression vector. P Natl Acad Sci USA. National Acad Sciences; 1985; 82: 3577–3581.

74. Lennox ES. Transduction of linked genetic characters of the host by bacteriophage P1. Virology. 1955; 1: 190–206. PMID: 13267987

75. Clark DJ, Maaløe O. DNA replication and the division cycle in Escherichia coli. J Mol Biol. 1967.

76. Hale CA, de Boer PA. Recruitment of ZipA to the septal ring of Escherichia coli is dependent on FtsZ and independent of FtsA. J Bacteriol. 1999; 181: 167–176. PMID: 9864327